A temperate former West Antarctic ice sheet suggested by an extensive zone of subglacial meltwater channels

Kathryn C. Rose[1]*, Neil Ross[2], Robert G. Bingham[3], Hugh F.J. Corr[4], Fausto Ferraccioli[4], Tom A. Jordan[4], Anne M. Le Brocq[5], David M. Rippin[6], and Martin J. Siegert[7]*

[1]Bristol Glaciology Centre, School of Geographical Sciences, University of Bristol, Bristol BS8 1SS, UK
[2]School of Geography, Politics & Sociology, Newcastle University, Newcastle NE1 7RU, UK
[3]School of Geosciences, University of Edinburgh, Edinburgh EH8 9XP, UK
[4]British Antarctic Survey, Cambridge CB3 0ET, UK
[5]School of Geography, University of Exeter, Exeter EX4 4RJ, UK
[6]Environment Department, University of York, York YO10 5DD, UK
[7]Grantham Institute and Department of Earth Science and Engineering, Imperial College London, London SW7 2AZ, UK

ABSTRACT

Several recent studies predict that the West Antarctic Ice Sheet will become increasingly unstable under warmer conditions. Insights on such change can be assisted through investigations of the subglacial landscape, which contains imprints of former ice-sheet behavior. Here, we present radio-echo sounding data and satellite imagery revealing a series of ancient large sub-parallel subglacial bed channels preserved in the region between the Möller and Foundation Ice Streams, West Antarctica. We suggest that these newly recognized channels were formed by significant meltwater routed along the ice-sheet bed. The volume of water required is likely substantial and can most easily be explained by water generated at the ice surface. The Greenland Ice Sheet today exemplifies how significant seasonal surface melt can be transferred to the bed via englacial routing. For West Antarctica, the Pliocene (2.6–5.3 Ma) represents the most recent sustained period when temperatures could have been high enough to generate surface melt comparable to that of present-day Greenland. We propose, therefore, that a temperate ice sheet covered this location during Pliocene warm periods.

INTRODUCTION

The marine-based West Antarctic Ice Sheet (WAIS) is considered highly susceptible to ocean and climate warming (Pritchard et al., 2012; Joughin et al., 2014), experiencing numerous oscillations since its formation (Naish et al., 2009). In order to assess the extent to which past changes to the WAIS are representative of its future behavior, it is important to understand the glaciological processes involved in those changes. Central to this is an appreciation of climate and ice-flow regimes, in particular the manner in which former ice sheets responded to a warmer climate. Greenland today provides useful examples of surface melting (Mote, 2007) influencing ice flow (Shepherd et al., 2009; Bartholomew et al., 2010, 2011).

Geomorphological analyses of subglacial topography have played a key role in reconstructing the nature of former ice masses in Antarctica (Young et al., 2011), as landscape evolution can be linked to glacial processes (Sugden and John, 1976, p.192–209). While radio-echo sounding (RES) is the primary tool used to map topography beneath modern ice sheets (Fretwell et al., 2013), satellite imagery of the ice surface has been shown to provide insights where RES is unavailable (Ross et al., 2014). Using this combination of data sets, we have identified a series of large (kilometer-scale), linear subglacial features, which we interpret as preserved, ancient subglacial meltwater channels. We assess the geometry of these channels in the context of their geographic location and the present-day hydrological setting of the ice sheet. We then infer the mechanism for their formation and suggest the most recent time at which this may have occurred, based on the climatic conditions required to support substantial, sustained subglacial meltwater routing at the ice-sheet bed. Our findings

have implications for the processes driving former ice-sheet oscillations and the response of the WAIS to warmer climatic conditions.

METHODS

Mapping of the bed topography across the study area is derived from a detailed RES survey of the Institute and Möller Ice Streams and Bedmap2 (Fretwell et al., 2013; Ross et al., 2014). The former data set was acquired using a coherent system with a 12 MHz bandwidth and 150 MHz carrier frequency (Ross et al., 2012), providing an ~10 m along-track sampling interval. Differential GPS, with a horizontal accuracy of ~5 cm, was used for positioning and to determine the elevation of the ice-sheet surface. Bed elevations were calculated by subtracting ice thickness measurements from ice surface elevations. In combination with Bedmap2, data were then rendered onto a 1-km-grid mesh, using the Topo to Raster function in ArcGIS (http://www.esri.com/software/arcgis; see the GSA Data Repository[1]).

The Moderate-Resolution Imaging Spectroradiometer (MODIS) Mosaic of Antarctica was used to examine the ice-sheet surface (Haran et al., 2005 [updated 2013]). Brightness variations in the image radiometry produce a detailed picture of the morphology of the ice-sheet surface (see the Data Repository), which was used to map surface features and provide information on subglacial topography.

RESULTS

RES data and satellite imagery reveal preserved, major subglacial channels incised into subglacial topography in the region between the Möller and Foundation Ice Streams (MIS and FIS, respectively) in West Antarctica (Fig. 1; Figs. DR1 and DR2 in the Data Repository). Topography in this region is characterized by hills and valleys, predominantly lies below sea level (mean of −585 m, range of −700 to 300 m), and marks the geological boundary between West and East Antarctica (Jordan et al., 2013). In the upper MIS catchment, there are six elongate subglacial basins, known as the Marginal Basins (Fig. 1C). The boundaries of these basins are associated with magnetic lineaments and Jurassic intrusions, some of which form nunataks (Jordan et al., 2013). The channels are located adjacent to these basins, beneath presently slow-flowing (<10 m yr^{-1}; Rignot et al., 2011), thin (≤1 km) and therefore cold-based (non-erosive) ice, providing appropriate conditions under which basal topographic features may be preserved (Sugden and John, 1976, p.192–209) and visible in surface imagery (Ross et al., 2014).

RES data show that channel cross-profiles are broad (average width of 2.6 km) and relatively shallow (average depth of 158.9 m), with an average elevation of –623 m (Figs. 2A–2D; Table DR1 in the Data Repository).
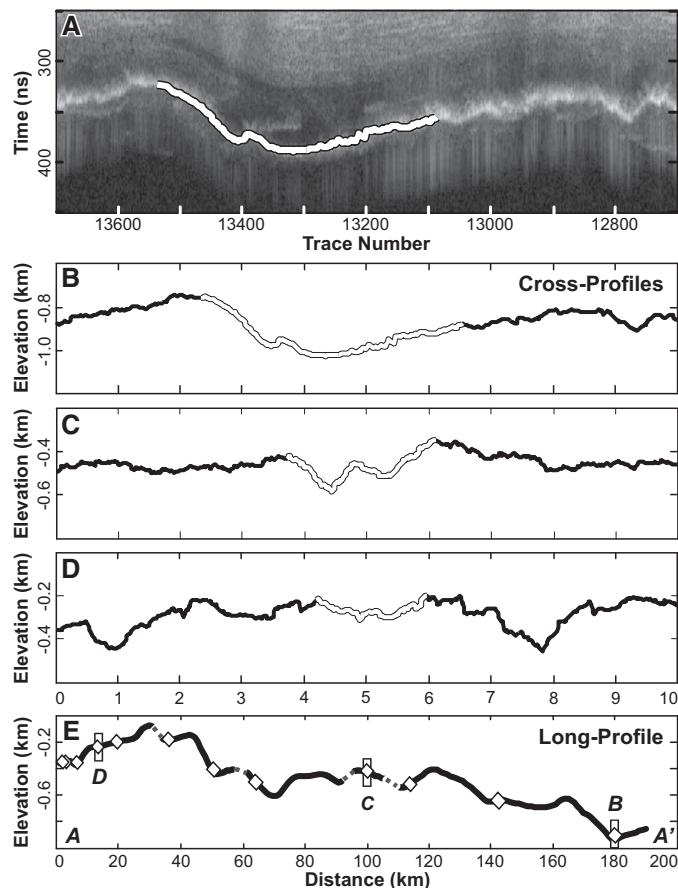
*E-mails: k.c.rose@bristol.ac.uk; m.siegert@imperial.ac.uk.
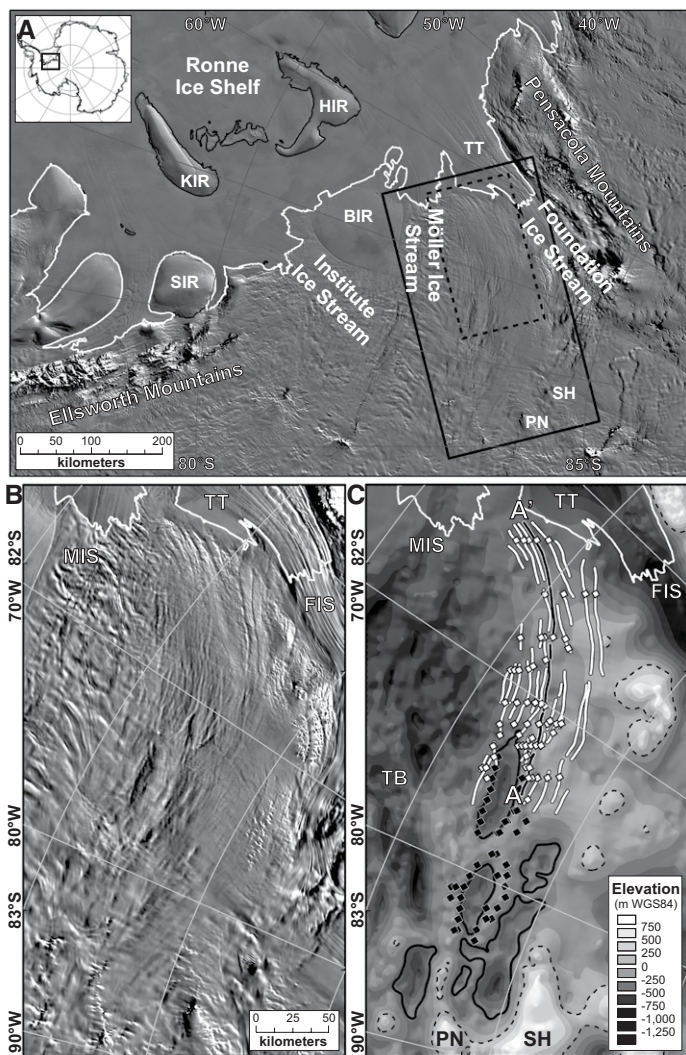
Figure 1. A: Moderate Resolution Imaging Spectroradiometer (MODIS) Mosaic of Antarctica satellite imagery showing location of study area within the inner Weddell Sea embayment, West Antarctica. Black box marks extent of B and C. Dashed black box is examined in Figs. DR2 and DR4 (see footnote 1). B: Linear surface features identified in MODIS imagery. C: Subglacial topography overlain with channel locations (white lines) observed in MODIS imagery (in B) on bed topography. Among these channels, the black line (A-A′) marks the channel long-profile plotted in Figure 2E. White diamonds identify subglacial channels that are visible in both MODIS imagery and radio-echo sounding (RES) data. Black diamonds mark channels only visible in RES data. Black dashed line is the 0 m elevation contour. Solid black lines are the Marginal Basins (–650 m contour). BIR—Bungenstock Ice Rise; FIS—Foundation Ice Stream; HIR—Henry Ice Rise; KIR—Korff Ice Rise; MIS—Möller Ice Stream; PN—Pagano Nunatak; SIR—Skytrain Ice Rise; SH—Stewart Hills; TB—Transitional Basins; TT—Thiel Trough.

Figure 2. Long- and cross-profiles from an example channel network. A: Example radar echogram showing the cross-profile plotted in B. B–D: Channel cross-profiles derived from flight-line data (vertical exaggeration of ~1:5×). White segments mark interpreted channel width along the black line, which records bed elevation. Cross-profile locations correspond with white horizontal lines shown in Fig. DR4A (see footnote 1). Cross-profiles are displayed looking downstream toward the grounding line (i.e., Möller Ice Stream on left, Foundation Ice Stream on right). E: Long-profile of channel floor elevations (vertical exaggeration of 1:25×) (Fig. 1C, black line A-A′). Vertical boxes mark locations of cross-profiles in B–D. White diamonds show intersections with flight-line data.

In MODIS imagery (Haran et al., 2005 [updated 2013]), the underlying channels are expressed as linear features in the ice-sheet surface (Fig. 1B), in regions where ice velocities fall below 10 m yr^{-1} (Rignot et al., 2011; Fig. DR3). We mapped 32 linear to sinuous channels, oriented independently of ice surface slope (Fig. 1C). The channels are evident as far as ~200 km inland from the grounding line, but are discontinuous in the satellite imagery, with average segment lengths of 42 km (Fig. DR4A). Over short (~5 km) distances, however, it is reasonable to extrapolate across the data gap with confidence so that, in some instances, combinations of segments can be classified as single channels (see the Data Repository

text, and Fig. DR4B). Channel-floor long-profiles reveal an irregular form, with several "reverse" (i.e., upstream/inland dipping) sections (Fig. 2E; Fig. DR5). Overall, the persistence and coincidence of both surface and bed features between flight lines, and their consistent orientation, indicate that they are associated and continuous.

DISCUSSION

Channel Formation

Several lines of evidence suggest that the channels observed were formed subglacially. Crucially, the channels are located well below sea level, even if the topography is rebounded to account for the removal of the modern ice-sheet load (Fig. 2; Figs. DR2 and DR5), thus precluding a pre-glacial fluvial origin. The formation of individual, straight channel segments in bedrock, often in a sub-parallel arrangement, is typically associated with subglacial meltwater erosion, where the primary control on channel formation is ice movement ("ice-directed channels"; Sugden and John, 1976, p. 304). Furthermore, the channels track over present-day reverse slopes, across the subglacial upland, and toward the modern grounding line, forming an "up-and-down" profile (Fig. 2E). This is par-

ticularly indicative of a subglacial fluvial origin, whereby pressurized flow under ice can drive water over subglacial obstacles (Sugden and John, 1976, p. 308). Indeed, we find evidence from RES data for water driven over topographic highlands in Antarctica today (Wright et al., 2014). Second, the broad, shallow channel cross-profiles observed (Fig. 2) are indicative of meltwater cross-profiles, which are commonly many times wider than they are deep, rather than the parabolic or U-shaped forms typically associated with glacial erosion by ice (Sugden and John, 1976, p. 178). At the margins of Antarctica, similar-scale, linear channels incised in bedrock have been found and are associated with erosion by abundant volumes of meltwater (Nitsche et al., 2013, and references therein).

Subglacial Meltwater Source

Geothermal heating and/or subglacial frictional melting are insufficient to generate the magnitude of meltwater required to erode the scale of channels observed (Nitsche et al., 2013). Wingham et al. (2006) identified, from satellite observations of discrete ice-sheet surface elevation changes, a 1.8 km^3 water pulse issued from an East Antarctic lake and routed >200 km at the bed. Lewis et al. (2006) suggested that similar discharges in the past may have formed the channelized landscape of the Labyrinth, in the Wright Dry Valley, Antarctica. We note that no substantial subglacial lake is presently observed upstream of the channels, despite technological advances that have allowed most (if not all) of the largest Antarctic subglacial lakes to be identified (Wright and Siegert, 2012). Nonetheless, we cannot discount the possibility that the enclosed Marginal Basins (Fig. 1C), which are ~22 km across and just over 800 m deep, may have formed subglacial lakes in the past. Indeed, the coupled orientation and proximity of the channels to the lakes suggests that the two are likely related. However, the channels are evidence of an abundance of basal water, more than is likely from subglacial lake discharges alone. This is because, irrespective of the volume of stored basal water, the physical mechanism of lake drainage self-regulates water outputs, so that lakes may only drain a small proportion of their total volume before the drop in water level reduces pressure at the lake outlet and causes the ice above to draw down and reseal (Fowler, 2009). Thus, while subglacial lake filling and episodic drainage may have occurred as an interrelated component of the subglacial hydrological system, a continuous and significant meltwater input is required to drive channel formation. We suggest, therefore, that the channels result from significant meltwater inputs to the bed from the ice surface, as the simplest explanation.

In a setting analogous to present-day Greenland (Bartholomew et al., 2011), for example, seasonal surface meltwater generation (Mote, 2007) can provide the intermittent, large pulses of meltwater required for this scale of channel formation over time (Schoof, 2010; Cowton et al., 2012). Formation of subglacial channels is likely to occur in association with enhanced ice-flow units, such as ice streams and outlet glaciers (Bartholomew et al., 2010). We note that in such regions of the Greenland Ice Sheet, surface melt rates, surface slopes, and ice-flow velocities are too high (Bamber et al., 2013) to retain a surface expression of subglacial channels, thus explaining their apparent absence in Greenland Ice Sheet surface imagery. However, as ice velocities are low across the studied region of the WAIS today, a surface expression of these channels has developed (Rignot et al., 2011).

Timing and Process of Channel Formation

We consider that channel development under present-day Antarctic ice-sheet conditions is not possible for six reasons.

(1) The channel orientations are not consistent with today's ice-surface contours (Fretwell et al., 2013) and, thus, the hydrological potential pathways for the region (Le Brocq et al., 2013) (see the Data Repository text, and Fig. DR6). Instead, channel orientation indicates that they formed under a different ice-sheet configuration and have since been preserved. During their formation, meltwater, and presumably ice flow,

drained toward the Thiel Trough (Fig. 1C; Fig. DR6). We have confidence that the locations of modeled pathways under present ice-sheet conditions are robust, given that they correspond with active meltwater outlets at the grounding line (Le Brocq et al., 2013).

(2) As we see no RES evidence for water in the channels (Fig. DR1) and the overlying ice is thin (<1 km), we believe that the ice sheet is frozen to the bed today.

(3) The inference of cold-based conditions is supported by the low ice velocities (2–10 m yr^{-1}) in this region (Rignot et al., 2011). If large quantities of meltwater were present, we might expect higher velocities and/or more dynamic ice flow. However, the majority of present-day ice flow (and the direction of hydraulic potential pathways) is focused along the MIS and FIS, which flank the channelized region (Figs. DR3 and DR6).

(4) There is no obvious source for subglacial water in the region today (Wright and Siegert, 2012). Antarctica is characterized by a polar desert climate where (with the exception of the Antarctic Peninsula and other coastal regions with ice shelves) surface melt rates are predominantly very low (<25 mm w.e. [water equivalent] yr^{-1}) (Trusel et al., 2013). Therefore, under present conditions, any surface melt that is produced refreezes. Although subglacial meltwater may be produced at pressure under thick (>2 km) ice, such thicknesses are not recorded here, and in the absence of a large subglacial lake, irrespective of the likely drainage mechanism, the quantity of stored water at the bed today is insufficient to erode channels of the scale observed.

(5) There is no indication of a significant, active, meltwater outlet corresponding to the location of the channels at the grounding line (Le Brocq et al., 2013).

(6) ICESat (Ice, Cloud, and Land Elevation Satellite) shows no evidence for ice surface elevation change associated with these channels (Smith et al., 2009), as might be expected if subglacial lake drainage were occurring (Wingham et al., 2006).

Consequently, we believe that supraglacial meltwater is the most likely driver of basal channel formation (Cowton et al., 2012).

The process of large-scale surface melting, leading to englacial transfer of water and basal flow (Shepherd et al., 2009; Bartholomew et al., 2011), requires temperate climate conditions. In such a setting, ice-sheet fluctuations are more equally controlled by a combination of atmospheric and oceanic changes, rather than the ocean-driven variations that dominate Antarctica today (Pritchard et al., 2012). Over the past 50 m.y., the world has experienced substantial global cooling, interspersed with marked periods of high warmth (Zachos et al., 2008). Of these warm periods, the Miocene (23–5.3 Ma) and, most recently, the Pliocene (5.3–2.6 Ma) are the most likely times in which surface ice-sheet melting was possible. While interglacials (e.g., marine isotope stage 11) are also warmer than today, they are likely cooler than these periods and relatively short in duration (on the order of thousands of years). In the Miocene, although the climate was adequately warm, the WAIS may not have been sufficiently well developed for large-scale grounded ice to form at this location for long periods (DeConto and Pollard, 2003). This, therefore, leaves the Pliocene as the most recent opportunity for the WAIS to have experienced Greenland-style behavior over a sustained time period.

During this period, global temperatures were generally 2–3 °C warmer (Dowsett, 2007) and sea level was, at times, up to 22 ± 10 m higher than present, implying a reduction in the size of both West and East Antarctic Ice Sheets (Miller et al., 2012). Indicative of such behavior, offshore sediments record fluctuations in WAIS extent. In particular, an early Pliocene 60-m-thick bed of diatomite in the ANDRILL (Antarctic Geological Drilling; http://www.andrill.org) core shows that the Ross Ice Shelf (and likely the West Antarctic Ice Sheet) disappeared for a period of over 200,000 yr and several glacial cycles (Naish et al., 2009, p. 323). Similarly, dynamic change is recorded at the margins of the East Antarctic Ice Sheet (EAIS) (Cook et al., 2013). Recent models of ice volume change for the late Pliocene–early Pleistocene have attributed this EAIS

behavior to summer melting at the ice-sheet margin (Raymo et al., 2006). Using glaciological and sea-level studies, the mass balance of the EAIS was shown to be comparable to that of today's Greenland Ice Sheet, where mean annual surface temperatures of −2 °C to −8 °C can accommodate ablation via both calving and summer surface melt (Raymo et al., 2006, their figure 3). Consequently, it follows that the WAIS would be subject to the same principles of summer insolation–driven surface melt and mass-balance processes. This suggests that the raised global temperatures of the Pliocene were capable of allowing meltwater to form and pond seasonally at the WAIS surface. This, in turn, indicates that the WAIS was characterized by temperate ice-sheet conditions during this time. In a setting similar to today's Greenland Ice Sheet, surface meltwater could have thereby reached the subglacial environment via englacial routing (Bartholomew et al., 2011) to erode the subglacial meltwater channels observed (Cowton et al., 2012). Importantly, we note that the channels are located >500 m below sea level today and would remain below sea level even with the removal of the modern ice-sheet load (Fig. DR2). Consequently, the temperate ice sheet responsible for their formation must have been marine based, at least in the study region (noting that we cannot extrapolate to the whole of the WAIS).

CONCLUSIONS

Using a combination of RES data and satellite imagery we have identified a series of subglacial meltwater channels incised into the bed between the Möller and Foundation Ice Streams, West Antarctica. We envisage that these channels formed under temperate ice-sheet conditions, when large volumes of supraglacial water was routed to the bed, whereupon it was driven by ice overburden to the margin, forming and further incising the channels by fluvial erosion. The most recent time when sustained surface melting could have taken place in Antarctica is the Pliocene. If this interpretation is correct, it means that ice was still present (at least periodically) in this location during the Pliocene and, potentially, the Miocene.

REFERENCES CITED

Bamber, J.L., et al., 2013, A new bed elevation dataset for Greenland: The Cryosphere, v. 7, p. 499–510, doi:10.5194/tc-7-499-2013.

Bartholomew, I., Nienow, P., Mair, D., Hubbard, A., King, M.A., and Sole, A., 2010, Seasonal evolution of subglacial drainage and acceleration in a Greenland outlet glacier: Nature Geoscience, v. 3, p. 408–411, doi:10.1038/ngeo863.

Bartholomew, I., Nienow, P., Sole, A., Mair, D., Cowton, T., Palmer, S., and Wadham, J., 2011, Supraglacial forcing of subglacial drainage in the ablation zone of the Greenland ice sheet: Geophysical Research Letters, v. 38, L08502, doi:10.1029/2011GL047063.

Cook, C.P., et al., 2013, Dynamic behaviour of the East Antarctic ice sheet during Pliocene warmth: Nature Geoscience, v. 6, p. 765–769, doi:10.1038/ngeo1889.

Cowton, T., Nienow, P., Bartholomew, I., Sole, A., and Mair, D., 2012, Rapid erosion beneath the Greenland ice sheet: Geology, v. 40, p. 343–346, doi:10.1130/G32687.1.

DeConto, R.M., and Pollard, D., 2003, Rapid Cenozoic glaciation of Antarctica induced by declining atmospheric CO_2: Nature, v. 421, p. 245–249, doi:10.1038/nature01290.

Dowsett, H.J., 2007, The PRISM palaeoclimate reconstruction and Pliocene sea-surface temperature, in Williams, M., et al., eds., Deep-Time Perspectives on Climate Change: Marrying the Signal from Computer Models and Biological Proxies: Geological Society of London, Micropalaeontological Society Special Publication, p. 459–480.

Fowler, A.C., 2009, Dynamics of subglacial floods: Proceedings of the Royal Society of London, Series A, v. 465, p. 1809–1828, doi:10.1098/rspa.2008.0488.

Fretwell, P., et al., 2013, Bedmap2: Improved ice bed, surface and thickness datasets for Antarctica: The Cryosphere, v. 7, p. 375–393, doi:10.5194/tc-7-375-2013.

Haran, T., Bohlander, J., Scambos, T., Painter, T., and Fahnestock, M., 2005 [updated 2013], MODIS Mosaic of Antarctica (MOA) Image Map, Map NSIDC_0280, MOA125_2004: Boulder, Colorado, National Snow and Ice Data Center, doi:10.7265/N5ZK5DM5.

Jordan, T.A., Ferraccioli, F., Ross, N., Corr, H.F.J., Leat, P.T., Bingham, R.G., Rippin, D.M., le Brocq, A., and Siegert, M.J., 2013, Inland extent of the Weddell Sea Rift imaged by new aerogeophysical data: Tectonophysics, v. 585, p. 137–160, doi:10.1016/j.tecto.2012.09.010.

Joughin, I., Smith, B.E., and Medley, B., 2014, Marine ice sheet collapse potentially under way for the Thwaites Glacier Basin, West Antarctica: Science, v. 344, p. 735–738, doi:10.1126/science.1249055.

Le Brocq, A.M., et al., 2013, Evidence from ice shelves for channelized meltwater flow beneath the Antarctic Ice Sheet: Nature Geoscience, v. 6, p. 945–948, doi:10.1038/ngeo1977.

Lewis, A.R., Marchant, D.R., Kowalewski, D.E., Baldwin, S.L., and Webb, L.E., 2006, The age and origin of the Labyrinth, western Dry Valleys, Antarctica: Evidence for extensive middle Miocene subglacial floods and freshwater discharge to the Southern Ocean: Geology, v. 34, p. 513–516, doi:10.1130/G22145.1.

Miller, K.G., Wright, J.D., Browning, J.V., Kulpecz, A., Kominz, M., Naish, T.R., Cramer, B.S., Rosenthal, Y., Peltier, W.R., and Sosdian, S., 2012, High tide of the warm Pliocene: Implications of global sea level for Antarctic deglaciation: Geology, v. 40, p. 407–410, doi:10.1130/G32869.1.

Mote, T.L., 2007, Greenland surface melt trends 1973–2007: Evidence of a large increase in 2007: Geophysical Research Letters, v. 34, L22507, doi:10.1029/2007GL031976.

Naish, T., et al., 2009, Obliquity-paced Pliocene West Antarctic ice sheet oscillations: Nature, v. 458, p. 322–328, doi:10.1038/nature07867.

Nitsche, F.O., Gohl, K., Larter, R.D., Hillenbrand, C.-D., Kuhn, G., Smith, J.A., Jacobs, S., Anderson, J.B., and Jakobsson, M., 2013, Paleo ice flow and subglacial meltwater dynamics in Pine Island Bay, West Antarctica: The Cryosphere, v. 7, p. 249–262, doi:10.5194/tc-7-249-2013.

Pritchard, H.D., Ligtenberg, S.R.M., Fricker, H.A., Vaughan, D.G., van den Broeke, M.R., and Padman, L., 2012, Antarctic ice-sheet loss driven by basal melting of ice shelves: Nature, v. 484, p. 502–505, doi:10.1038/nature10968.

Raymo, M.E., Lisiecki, L.E., and Nisancioglu, K.H., 2006, Plio-Pleistocene ice volume, Antarctic climate, and the global $\delta^{18}O$ record: Science, v. 313, p. 492–495, doi:10.1126/science.1123296.

Rignot, E., Mouginot, J., and Scheuchl, B., 2011, Ice flow of the Antarctic Ice Sheet: Science, v. 333, p. 1427–1430, doi:10.1126/science.1208336.

Ross, N., Bingham, R.G., Corr, H.F.J., Ferraccioli, F., Jordan, T.A., Le Brocq, A., Rippin, D.M., Young, D., Blankenship, D.D., and Siegert, M.J., 2012, Steep reverse bed slope at the grounding line of the Weddell Sea sector in West Antarctica: Nature Geoscience, v. 5, p. 393–396, doi:10.1038/ngeo1468.

Ross, N., Jordan, T.A., Bingham, R.G., Corr, H.F.J., Ferraccioli, F., Le Brocq, A., Rippin, D.M., Wright, A.P., and Siegert, M.J., 2014, The Ellsworth Subglacial Highlands: Inception and retreat of the West Antarctic Ice Sheet: Geological Society of America Bulletin, v. 126, p. 3–15, doi:10.1130/B30794.1.

Schoof, C., 2010, Ice-sheet acceleration driven by melt supply variability: Nature, v. 468, p. 803–806, doi:10.1038/nature09618.

Shepherd, A., Hubbard, A., Nienow, P., King, M., McMillan, M., and Joughin, I., 2009, Greenland ice sheet motion coupled with daily melting in late summer: Geophysical Research Letters, v. 36, L01501, doi:10.1029/2008GL035758.

Smith, B.E., Fricker, H.A., Joughin, I.R., and Tulaczyk, S., 2009, An inventory of active subglacial lakes in Antarctica detected by ICESat (2003–2008): Journal of Glaciology, v. 55, p. 573–595, doi:10.3189/002214309789470879.

Sugden, D.E., and John, B.S., 1976, Glaciers and Landscape: London, Edward Arnold.

Trusel, L.D., Frey, K.E., Das, S.B., Munneke, P.K., and van den Broeke, M.R., 2013, Satellite-based estimates of Antarctic surface meltwater fluxes: Geophysical Research Letters, v. 40, p. 6148–6153, doi:10.1002/2013GL058138.

Wingham, D.J., Siegert, M.J., Shepherd, A., and Muir, A.S., 2006, Rapid discharge connects Antarctic subglacial lakes: Nature, v. 440, p. 1033–1036, doi:10.1038/nature04660.

Wright, A., and Siegert, M., 2012, A fourth inventory of Antarctic subglacial lakes: Antarctic Science, v. 24, p. 659–664, doi:10.1017/S095410201200048X.

Wright, A.P., Young, D.A., Bamber, J.L., Dowdeswell, J.A., Payne, A.J., Blankenship, D.D., and Siegert, M.J., 2014, Subglacial hydrological connectivity within the Byrd Glacier catchment, Antarctica: Journal of Glaciology, v. 60, p. 345–352, doi:10.3189/2014JoG13J014.

Young, D.A., et al., 2011, A dynamic early East Antarctic Ice Sheet suggested by ice-covered fjord landscapes: Nature, v. 474, p. 72–75, doi:10.1038/nature10114.

Zachos, J.C., Dickens, G.R., and Zeebe, R.E., 2008, An early Cenozoic perspective on greenhouse warming and carbon-cycle dynamics: Nature, v. 451, p. 279–283, doi:10.1038/nature06588.

Supplementary Information

1. Bed topography digital elevation model

Bed topography across the study area is derived from a detailed aerogeophysical survey (Fig. 1A, black lines) of the Institute and Möller Ice Streams (IMIS) and a series of individual flightlines flown in the 1970s (Fig. 1A, black dashed lines). Bedmap2 provides a grid of Antarctica's bed topography that incorporates these datasets, but does not provide access to the raw data (Fretwell et al., 2013). Although the data is rendered at a 1 km resolution, Bedmap2 bed topography is only really effective at a 5 km grid resolution due to the distribution of direct measurements (Fretwell et al., 2013). This work, however, is funded by the NERC AFI project that surveyed the IMIS. Therefore, the raw flightline data can be used in the gridding process, rather than the Bedmap2 data, in order to produce a more detailed grid of subglacial topography for this region. This was achieved using standard geoprocessing tools in the Spatial Analyst Toolbox in ArcGIS, as outlined below.

   The IMIS flightline data records elevations relative to WGS84. Therefore, a correction was applied to Bedmap2 to convert elevations from meters relative to sea level as defined by the g104c geoid to WGS84 datum heights. This involved subtracting the correction grid provided from the Bedmap2 grid (Fretwell et al., 2013). A section of the grid, encompassing the study area under investigation (Fig. 1), was then extracted from Bedmap2 and converted to points. Each point represents the bed elevation value at the centre of a 5 km grid cell. A cubic convolution algorithm was used to determine this elevation. Bedmap2 elevation data were then deleted where they coincide with IMIS flightline data. The IMIS survey points are then gridded with the Bedmap2 points for the study area, at a 1 km resolution, using the 'Topo to Raster' function in ArcGIS. This uses an iterative finite difference interpolation technique that employs a nested grid strategy to calculate successively finer grids until the user specified resolution is obtained (Hutchinson 1988a,b). This technique has been widely used as the algorithm has been shown to represent glaciated landscapes well and was employed in the creation of Bedmap2 (Fretwell et al., 2013). The resulting grid was used as the basis of analysis for this paper, except where it was possible to use bed elevations directly from the IMIS flightline data (e.g. channel cross-profiles).

2. MODIS MOA image map

The Moderate Resolution Imaging Spectroradiometer (MODIS) comprises visible and near-infrared satellite sensors, which measure brightness variations in Bands 1 and 2. The Mosaic of Antarctic (MOA) image map (2004) consists of 260 MODIS orbit swaths, and represents a composite of digitally smoothed red-light (MODIS Band 1) images, at a resolution of 125 m (Haran et al., 2005, updated 2013). The processing steps involved mean that the final image is a consistent and semi-quantitative representation of red-light reflections. Brightness variations in the image radiometry produce a detailed picture of the morphology of the ice sheet surface (Scambos et al., 2007). This, in

turn, provides information on ice flow, subglacial bedrock form, wind-derived features and the location of the ice sheet grounding line.

3. Extracting channel long-profiles

A total of 44 discontinuous linear features were identified in satellite imagery (Fig. 1; Fig. DR4). These were interpreted as the surface expression of channel segments in the underlying bed topography. In order to determine the long-profile elevations of these channel segments, their locations in MODIS MOA satellite imagery (Haran et al., 2005, updated 2013) were first digitised in ArcGIS (Fig. DR4A, green lines). Once digitised, the pattern and spatial connectivity between channel segments became more evident. For some channels and over short distances, it was possible to extrapolate between channel segments with confidence and, therefore, to reclassify these segments as one channel. This resulted in the classification of a total of 32 single channels (Fig. DR4B). The location and length of each digitised channel was recorded. Then, in order to determine the channel long-profile elevations, each channel segment was converted into equally spaced points, at 1 km intervals along each line. Bed elevations at each point were then sampled directly from the flightline data (where the two intersected) or from the grid of subglacial topography (see Supplementary Information #1). The long-profiles presented in Fig. DR5 are plots of these elevation values against distance along the segment length. The first point (0 km) is always the most southerly, with each subsequent point located further north, towards the grounding line, with distance along the profile. The black dots mark where bed elevations were taken from intersecting flightline data. The dashed lines show where channel segments were grouped to represent a single channel long-profile.

4. Determining hydrological potential

Hydrological potential represents the gradient along which water will flow under ice (Shreve, 1972; Cuffey and Paterson, 2010). This incorporates flow resulting from a combination of elevation and pressure gradients (high to low). As such hydrological potential (ϕ_h) can be defined as:

$$\emptyset_h = P_w + (\rho_w * g * z)$$

Where water density (ρ_w) is 1000 kg m^{-3}, gravitational acceleration (g) is 9.81 m s^{-2}, elevation (z) is taken from the bed elevation grid and subglacial water pressure (P_w) is assumed to be equivalent to ice overburden pressure (σ), as follows:

$$\sigma = \rho_i * g * h_i$$

where ρ_i is density of ice (917 kg m^{-3}), g is gravitational acceleration and h_i is ice thickness. This allows hydrological potential to be re-written (Shreve, 1972) as:

$$\emptyset_h = \sigma + (\rho_w * g * z)$$

In order to solve this equation two grids are created in ArcGIS, as follows:

$$GridA = \rho_i * g * h_i$$

$$GridB = \rho_w * g * z$$

The ice thickness and bed elevation values used in these calculations are derived from Bedmap2 grids (1 km resolution) (Fretwell et al., 2013). The hydrological potential gradient is then determined by adding these two grids together, resulting in 1 km gridded surface of hydrological potential.

This hydrological potential grid is then employed as the primary input to ArcGIS's Hydrology Toolbox, which is used to determine the flow of water across a surface and thereby, derive the hydrological potential flow paths. In this process, flow direction is determined, hydrological sinks are identified, flow accumulation is calculated (number of upslope cells flowing to a location) and hydrological networks are identified. These pathways represent where water would flow, if present, beneath the ice sheet (Fig. DR6).

References

Fretwell, P., *et al.* 2013, Bedmap2: improved ice bed, surface and thickness datasets for Antarctica: The Cryosphere, v. 7, p. 375-393.

Hutchinson, M. F., 1988a, Calculation of hydrologically sound digital elevation models, *in* Proceedings of the Third International Symposium on Spatial Data Handling, p. 117–133.

Hutchinson, M. F., 1988b, A new procedure for gridding elevation and streamline data with automatic removal of spurious pits: Journal of Hydrology, v. 106, p. 211–232.

Haran, T., Bohlander, J., Scambos, T., Painter, T., and Fahnestock, M., 2005, updated 2013, MODIS Mosaic of Antarctica (MOA) Image Map [NSIDC_0280, MOA125_2004]: Boulder, Colorado USA: National Snow and Ice Data Center, http://dx.doi.org/10.7265/N5ZK5DM5.

Scambos, T.A., Haran, T M., Fahnestock, M.A., Painter, T.H, and Bohlander, J., 2007, MODIS-based Mosaic of Antarctica (MOA) data sets: Continent-wide surface morphology and snow grain size: Remote Sensing of Environment, v. 111, no. 2-3, p. 242-257.

Shreve, R.L., 1972, Movement of water in glaciers: Journal of Glaciology, v. 11, no. 2, p. 205-214.

Cuffey K.M., and Patterson, W.S.B., 2010, The Physics of Glaciers (4th Edition): Butterworth-Heinemann, Oxford, UK.

Rignot, E., Mouginot, J., and Scheuchl, B., 2011, Ice flow of the Antarctic Ice Sheet: Science, v. 333, p. 1437-1430.
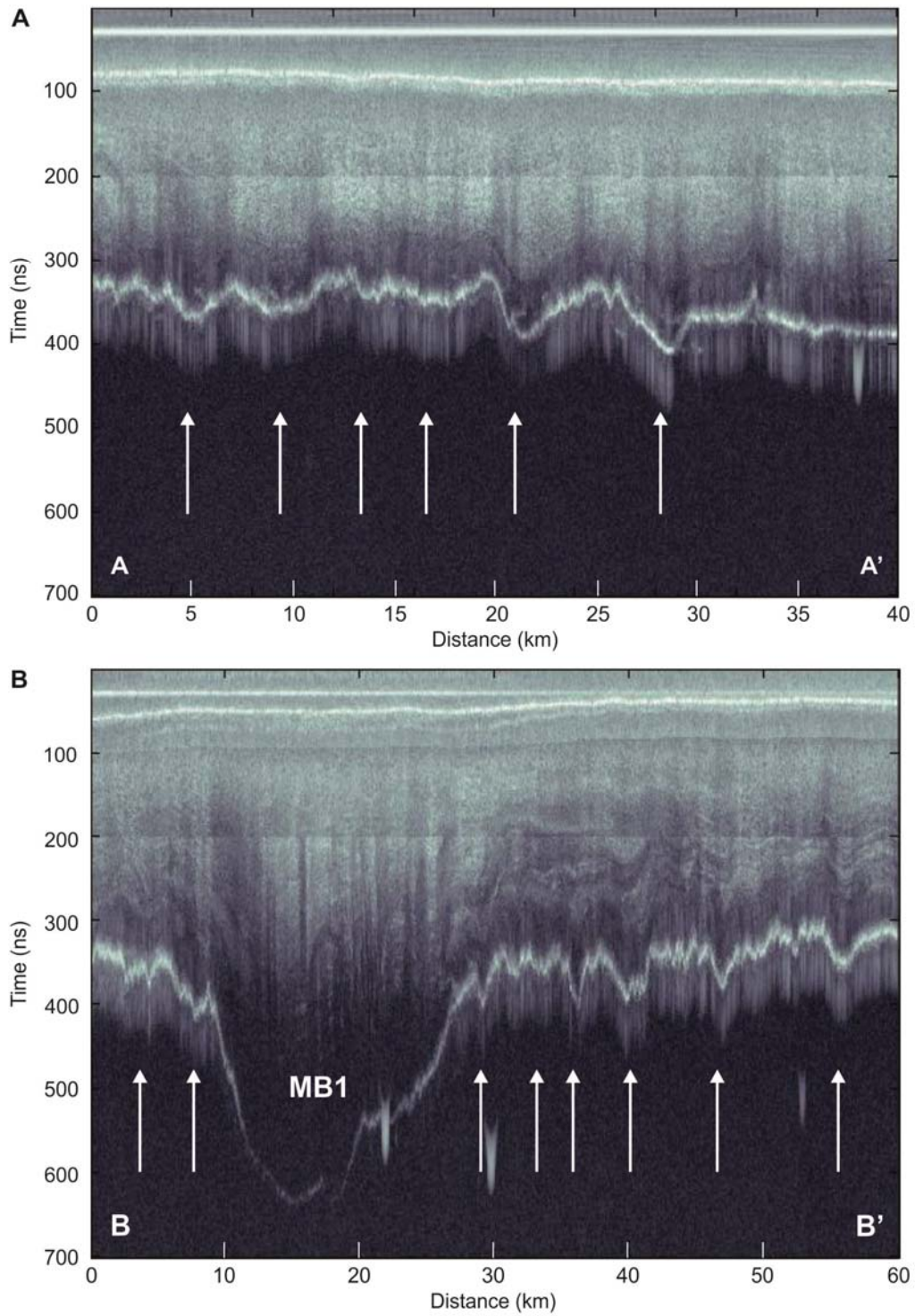
Figure DR1. Radar echograms showing examples of the subglacial channels identified. **A**: Radar echogram of transect A-A'. **B:** Radar echogram of transect B-B', which crosses the most northerly (down glacier) Marginal Basin 1. White arrows mark channel locations and correspond to the vertical dashed lines shown in the respective transects in Supplementary Fig. DR2.
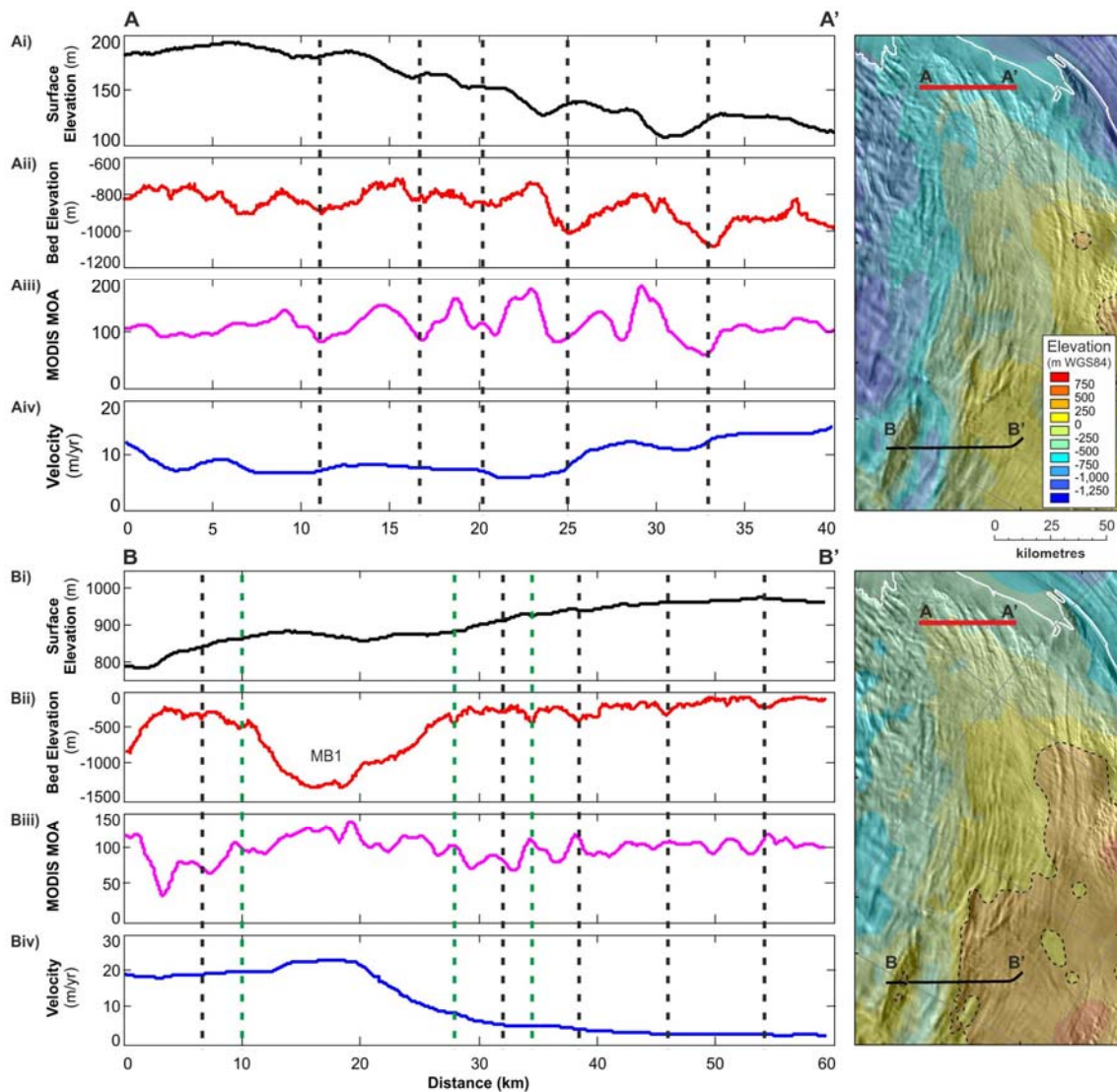
Figure DR2. Two transects taken along flightlines that cross a series of subglacial channels observed in RES data and satellite imagery in the region between the Möller and Foundation Ice Streams. **i,** Surface elevation. **ii,** Bed elevation. These are taken from the RES flightline data. **iii,** MODIS MOA satellite imagery (Haran et al., 2005, updated 2013). **iv,** Ice velocity (Rignot et al., 2011). These are sampled from grids. **A**: Flightline transect A-A' (red line) is located near the grounding line. **B**: Flightline transect B-B' (black line) is located further inland and crosses the northernmost (down glacier) Marginal Basin (Fig. 1C; Supplementary Fig. S1). Vertical black dashed lines mark the location of channels evident in the bed topography and at the ice sheet surface (Fig. 1C, white diamonds). Vertical green dashed lines mark the location of channels that are only evident in the bed topography (Fig. 1C, black diamonds). Inset: Present-day (upper) and rebounded (lower) bed elevations, overlain with a 0 m elevation contour, respectively (black dashed line), semi-transparent MODIS MOA imagery and associated grounding line (white line). Extent of inset is dashed black box in Fig. 1A.
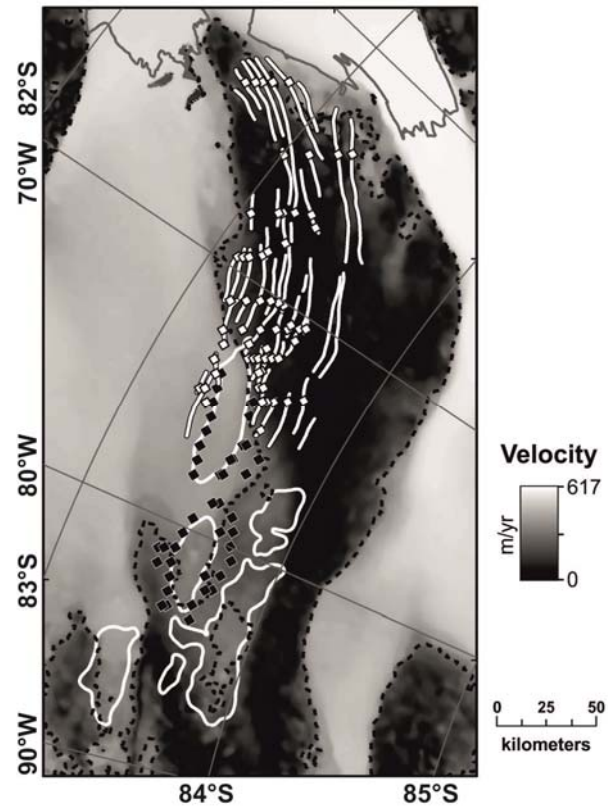
Figure DR3. Ice sheet velocity in the region of the Möller and Foundation Ice Streams, West Antarctica (Rignot et al., 2011). Dashed black line marks the 10 m a^{-1} contour. Grey line marks the MODIS MOA grounding line. White closed contours are the Marginal Basins (Fig. 1C). White lines show the location of channels observed in MODIS MOA imagery (Fig. 1B). White diamonds mark subglacial channels visible in both RES data and satellite imagery. Black diamonds mark subglacial channels only visible in RES data. Note: the surface expression of channels in the satellite imagery (white lines) closely corresponds with the 10 m a^{-1} velocity contour. Where ice sheet velocities are equal to or lower than this, the channels are evident in satellite imagery. Where ice sheet velocities exceed 10 m a^{-1} the channels are no longer visible at the ice surface.
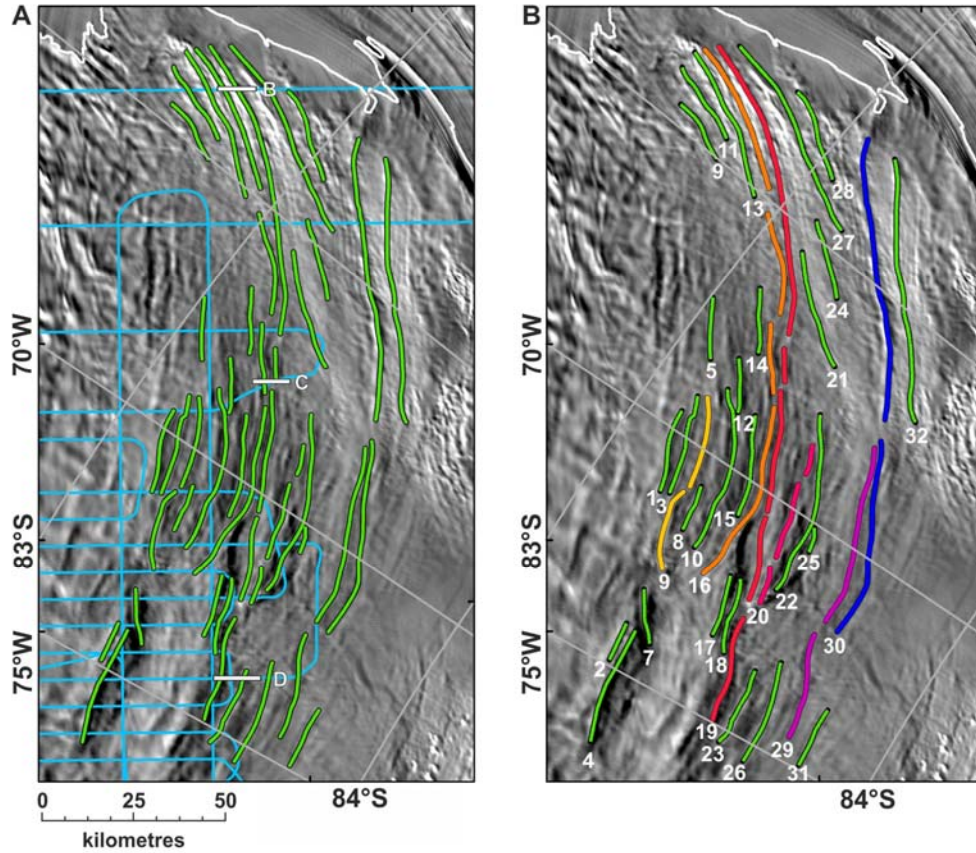
Figure DR4. Location and classification of channels observed in MODIS MOA imagery (Haran et al., 2005, updated 2013). Extent of panels is dashed black box in Fig. 1A. **A:** Green lines mark the location of 44 discontinuous channel segments identified in the MODIS MOA imagery. Blue lines represent flightlines, to show the spatial overlap between the two. Short white lines on the flightlines and lettering mark the locations of cross-profiles displayed in Fig. 2. **B:** For some channels and over short distances it was reasonable to extrapolate between channel segments with confidence and reclassify these segments as one channel (Supplementary Information #3). This resulted in the classification of a total of 32 single channels, labelled accordingly in this panel. To highlight where this occurred, those segments reclassified as a single channel are displayed in the same colour.
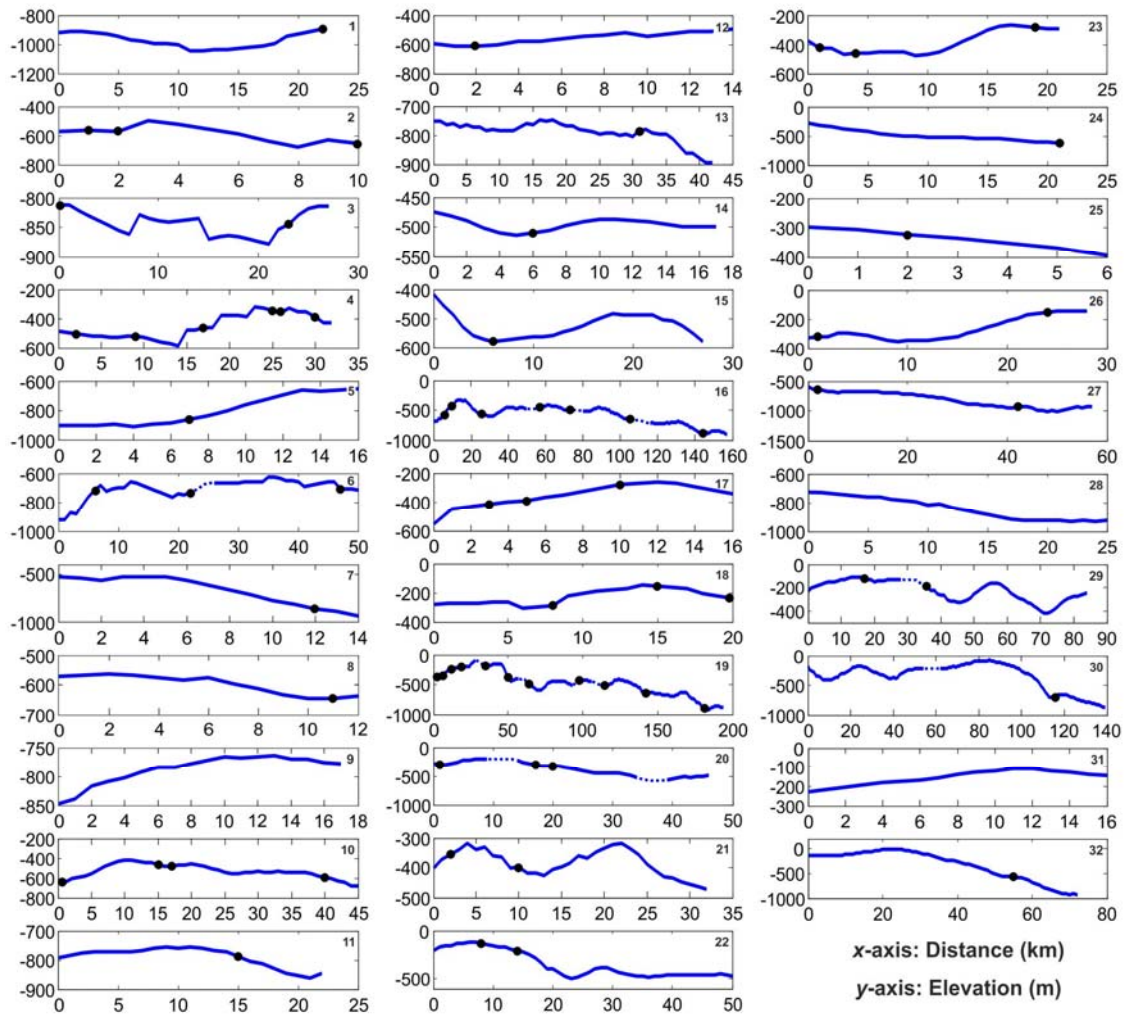
Figure DR5. Long-profiles of bed topography determined for the 32 channels identified in MODIS MOA imagery (Supplementary Fig. DR4). Elevations are derived from flightline data where channels intersected with flightlines (black dots) and elsewhere from the gridded bed topography (Supplementary Information #1 and 3). The long-profiles are numbered according to their corresponding channel segment detailed in Supplementary Fig. DR4B. Blue dashed lines mark extrapolated sections where channel segments were grouped into a single channel long-profile (i.e. channels 6, 16, 19, 20, 29 and 30). Note: the axes scales vary.
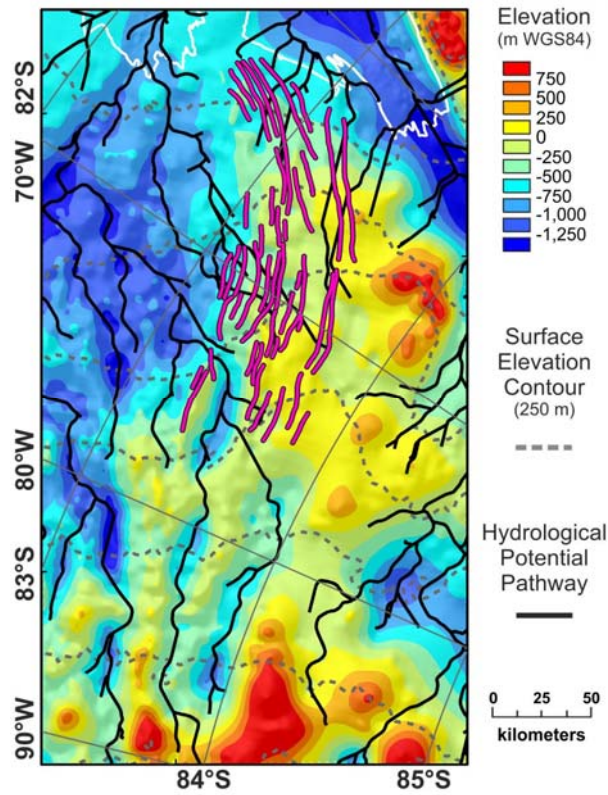
Figure DR6. Hydrological potential pathways and ice surface contours in the region of the Möller and Foundation ice streams, West Antarctica. Pathways (black lines) and surface contours (dashed grey lines, 250 m intervals) show where water would flow, if present beneath the ice sheet (Supplementary Information #4). Pink lines mark the location of channels observed in MODIS MOA satellite imagery (Fig. 1C). Channel orientations do not correspond with the direction of present-day hydraulic potential flow pathways and surface contours, indicating that they formed under a different ice sheet configuration and have since been preserved.

Table DR1. Example channel cross-profile dimensions and associated ice thicknesses.   A total of 103 cross-profiles were identified in RES data. These are marked by the diamonds shown in Fig. 1C. This table presents the data for the 60 white diamonds, which mark where channels at the bed coincide with channels identified in the MODIS MOA imagery. The associated MODIS channel ID number (Supplementary Fig. S4B) is listed alongside the cross-profile ID number. More than one cross-profile is often found along the length of the MODIS channels. The cross-profiles displayed in Fig. 2 are identified with additional letters B, C, and D and highlighted in grey. They are found along channel 19 (Fig. 2E).

ID		Elevation (m)			Depth (m)		Width	
Cross-Profile	Channel	West	Mid	East	Minimum	Maximum	m	km
1	6	-832.3	-1103.7	-835.1	268.6	271.4	8067.3	8.1
2	10	-812.0	-1027.9	-753.3	215.9	274.6	6351.4	6.4
3	16	-745.5	-883.2	-793.7	89.5	137.7	4650.7	4.7
4	19	-780.3	-851.4	-720.5	71.1	130.9	2318.9	2.3
5	20	-741.9	-920.7	-779.8	140.9	178.8	5968.7	6.0
6	22	-620.0	-842.8	-648.4	194.4	222.8	5354.2	5.4
7	25	-570.2	-800.3	-625.5	174.8	230.1	4471.7	4.5
8	26	-499.0	-948.8	-448.8	449.8	500.0	4963.1	5.0
9	23	-574.7	-835.3	-628.3	207.0	260.6	2228.1	2.2
10	19	-356.7	-543.9	-439.0	104.9	187.2	2077.2	2.1
11 (D)	19	-436.6	-652.1	-473.5	178.6	215.5	3412.8	3.4
12	4	-527.6	-646.2	-526.8	118.6	119.4	2340.2	2.3
13	16	-528.8	-596.1	-513.4	67.3	82.7	1678.6	1.7
14	24	-778.2	-947.9	-790.1	157.8	169.7	3405.2	3.4
15	30	-857.3	-928.2	-823.0	70.9	105.2	997.8	1.0
16	32	-799.1	-913.8	-761.7	114.7	152.1	2926.7	2.9
17	27	-719.5	-828.7	-689.7	109.2	139.0	1563.8	1.6
18 (B)	19	-532.4	-653.1	-530.0	120.7	123.1	3293.8	3.3
19	16	-484.5	-519.2	-443.7	34.7	75.5	734.2	0.7
20	13	-420.5	-586.9	-452.7	134.2	166.4	1055.1	1.1
21	11	-225.3	-369.1	-184.1	143.8	185.0	2179.0	2.2
22	1	-549.9	-724.0	-542.6	174.1	181.4	2090.1	2.1
23	3	-566.8	-730.6	-550.7	163.8	179.9	1916.2	1.9
24	6	-513.5	-602.8	-430.0	89.3	172.8	1850.9	1.9
25	10	-424.1	-509.8	-460.1	49.7	85.7	2359.7	2.4
26	12	-596.6	-719.2	-607.5	111.7	122.6	2200.2	2.2
27	16	-722.3	-926.3	-695.2	204.0	231.1	2404.7	2.4
28	21	-728.2	-833.4	-690.8	105.2	142.6	2126.1	2.1
29	21	-575.2	-718.6	-544.4	143.4	174.2	2014.3	2.0
30 (C)	19	-510.8	-616.4	-491.9	105.6	124.5	3025.4	3.0

Table DR1 continued. Example channel cross-profile dimensions and associated ice thicknesses.

Cross-Profile	Channel	West	Mid	East	Minimum	Maximum	m	km
		Elevation (m)			**Depth (m)**		**Width**	
31	16	-450.3	-700.0	-484.5	215.5	249.7	3684.5	3.7
32	14	-284.1	-357.3	-285.2	72.1	73.2	2651.8	2.7
33	5	-159.6	-285.1	-132.6	125.5	152.5	2426.5	2.4
34	7	-207.8	-381.9	-252.4	129.5	174.1	1853.4	1.9
35	17	-960.7	-1163.0	-927.0	202.3	236.0	3553.6	3.6
36	17	-653.7	-822.8	-583.4	169.1	239.4	2353.2	2.4
37	17	-121.3	-233.9	-174.7	59.2	112.6	1139.9	1.1
38	18	-803.2	-1012.1	-703.8	208.9	308.3	4466.4	4.5
39	19	-611.4	-748.7	-493.8	137.3	254.9	3007.4	3.0
40	20	-451.6	-517.6	-372.5	66.0	145.1	1691.8	1.7
41	22	-212.8	-259.5	-206.6	46.7	52.9	642.6	0.6
42	20	-106.1	-259.7	-161.9	97.8	153.6	2799.0	2.8
43	19	-183.6	-389.7	-212.7	177.0	206.1	2156.9	2.2
44	16	-275.1	-401.9	-268.4	126.8	133.5	1781.3	1.8
45	15	-209.7	-392.5	-233.1	159.4	182.8	1554.6	1.6
46	10	-233.5	-419.3	-275.0	144.3	185.8	1213.6	1.2
47	8	-510.6	-556.8	-502.9	46.2	53.9	785.6	0.8
48	3	-478.8	-557.0	-441.4	78.2	115.6	718.6	0.7
49	2	-385.4	-457.7	-313.7	72.3	144.0	653.0	0.7
50	4	-239.3	-332.7	-231.8	93.4	100.9	1391.8	1.4
51	18	-274.5	-334.0	-290.9	43.1	59.5	420.0	0.4
52	19	-75.4	-235.0	-72.4	159.6	162.6	3738.7	3.7
53	6	-171.4	-334.0	-159.6	162.6	174.4	2097.5	2.1
54	16	-182.3	-413.0	-205.0	208.0	230.7	3766.6	3.8
55	18	-227.5	-455.4	-258.4	197.0	227.9	1502.4	1.5
56	18	-202.1	-316.1	-214.5	101.6	114.0	1706.2	1.7
57	18	-291.8	-391.1	-312.4	78.7	99.3	810.6	0.8
58	7	-263.5	-445.8	-278.5	167.3	182.3	2118.7	2.1
59	23	-459.4	-759.1	-271.7	299.7	487.4	3661.8	3.7
60	29	-359.4	-635.3	-362.3	273.0	275.9	4710.9	4.7
Mean		-467.9	-622.5	-459.3	140.5	177.2	2584.7	2.6